Kinetic theory of a confined polymer driven by an external force and pressure-driven flow

Jason E. Butler,[a] O. Berk Usta, Rahul Kekre, and Anthony J. C. Ladd
Department of Chemical Engineering, University of Florida, Gainesville, Florida 32611, USA

(Received 6 June 2007; accepted 6 September 2007; published online 6 November 2007)

Kinetic theory is used to investigate the mechanisms causing cross-stream migration of confined polymers and polyelectrolytes under the influence of external forces and flow fields. Numerical simulations and experiments have demonstrated that confined polymers migrate towards the center of the channel in response to both external forces and uniaxial flows. Yet, migration towards the walls has been observed with combinations of external force and flow. In this paper, the kinetic theory for an elastic dumbbell developed by Ma and Graham [Phys. Fluids **17**, 083103 (2005)] has been extended to account for the effects of an external force. Further modifications account for counterion screening within a Debye-Hückel approximation. This enables qualitative comparison with experimental results [Zheng and Yeung, Anal. Chem. **75**, 3675 (2003)] on DNA migration under combined electric and pressure-driven flow fields. The comparison supports the contention [Long *et al.*, Phys. Rev. Lett. **76**, 3858 (1996)] that the hydrodynamic interactions in polyelectrolytes decay algebraically, as $1/r^3$, rather than exponentially. The theory qualitatively reproduces results of both simulations and experiments for the migration of neutral polymers and polyelectrolytes. Concentration profiles similar to those found in numerical simulations are observed, but the Peclet numbers differ by factors of 2–3. © *2007 American Institute of Physics*. [DOI: 10.1063/1.2801409]

I. INTRODUCTION

Macromolecules in solution exhibit a variety of phenomena during flow that can create concentration gradients within an initially homogeneous system.[1] The net migration of flexible polymers towards the center of a channel in response to pressure-driven flow is a well-studied case.[2–6] In pressure-driven flow, hydrodynamic lift on a polymer in the vicinity of a bounding wall causes the migration.[4,7] The local shear flow extends the polymer, generating tension in the chain and an additional flow field around the polymer. This flow field becomes asymmetric near a no-slip boundary and results in a net drift towards the center of the channel.

Recent simulations of a confined polymer driven by an external force also found migration towards the centerline,[8] though the mechanism clearly differs from shear-induced migration. Furthermore, simultaneous application of an external force and a pressure-driven flow altered the migration in a nonadditive fashion. When force and flow were applied in conjunction, the migration towards the centerline was enhanced. However, applying the external force in the opposite direction of the pressure-driven flow caused a migration either towards or away from the walls, depending upon the magnitude of the applied force.

In this paper, migration of a polymer chain under combinations of external force and pressure-driven flow is examined using the kinetic theory of an elastic dumbbell. The theory of Ma and Graham[7] is extended in Sec. II to include the action of the external force on the polymer. Results from the theory for different combinations of force and flow are presented and discussed in Sec. III. The theory qualitatively reproduces all the migration phenomena observed in the simulations. Multiple migration mechanisms having significant effects on the polymer distribution are identified.

The controllable, transverse migration of flexible macromolecules using combinations of imposed flow and an external force has potential applications to biotechnology; for example, the separation of DNA by size.[9] Here, an electric field acting upon the polyelectrolyte provides the external force leading to migration.[10] However, neither the simulations[8] nor the kinetic theory developed in Sec. II consider the effects of counterion screening on the hydrodynamic interactions induced by the electric field. Models of electrophoresis typically assume complete screening,[11] so that hydrodynamic interactions between polymer segments can be ignored. This free draining assumption is critical, since the relevant mechanisms identified in Sec. III result from hydrodynamic interactions. However, within the Debye-Hückel approximation, there remains a dipolar contribution to the hydrodynamic flow field around a screened point charge,[12,13] which was overlooked in the original work.[11] Moreover, experiments[14] on DNA in combined electric and pressure-driven flow fields measured nonuniform distributions of DNA transverse to the flow direction. The qualitative similarities between the experimental results, the numerical simulations,[8] and theory developed in Sec. II suggest that the screening of the velocity disturbance created by electrophoresis is not complete. Consequently, modifications to the theory are made in Sec. IV to account for the counterion screening of hydrodynamic interactions within the Debye-Hückel approximation. The results presented in Sec. IV D demonstrate that migration can occur

[a]Electronic mail: butler@che.ufl.edu

for combinations of electrophoresis and pressure-driven flow, and that hydrodynamic interactions in polyelectrolytes decay algebraically.

II. MODEL

The migration of polymers in dilute solution is examined using the kinetic theory for an elastic dumbbell. The analysis[7] for a polymer subjected to a local shear flow is extended to include both body forces and electric fields, using the same approximations: the polymer distribution function is factorized into a product of center-of-mass and orientation distributions, the effects of the no-slip boundary condition at the confining walls are superposed, and a far-field approximation for the hydrodynamic interactions with the bounding walls is made. Rather than numerically solving for the orientation distribution function,[7] the distribution is expanded in a power series in the force and flow fields. This additional approximation enables an analytic solution for the time independent distribution.

The evolution of a polymer dumbbell in solution can be described by a continuity equation for the distribution function, $\Psi(\mathbf{r}_c,\mathbf{q},t)$, of the center-of-mass $\mathbf{r}_c$ and end-to-end vector $\mathbf{q}$,[15]

$$\frac{\partial \Psi}{\partial t} = -\frac{\partial}{\partial \mathbf{r}_c}\cdot(\dot{\mathbf{r}}_c\Psi) - \frac{\partial}{\partial \mathbf{q}}\cdot(\dot{\mathbf{q}}\Psi). \tag{1}$$

The probability distribution function is separated into center-of-mass (n) and end-to-end (ψ) distribution functions,

$$\Psi(\mathbf{r}_c,\mathbf{q},t) = n(\mathbf{r}_c,t)\psi(\mathbf{r}_c,\mathbf{q},t), \tag{2}$$

where

$$n(\mathbf{r}_c,t) = \int \Psi(\mathbf{r}_c,\mathbf{q},t)d\mathbf{q}. \tag{3}$$

Integrating Eq. (1) over $\mathbf{q}$ gives the steady-state distribution of the center-of-mass,

$$\frac{\partial}{\partial \mathbf{r}_c}\cdot(n\langle\dot{\mathbf{r}}_c\rangle) = 0, \tag{4}$$

where the angle brackets $\langle\rangle$ indicate an ensemble average over $\mathbf{q}$,

$$\langle\dot{\mathbf{r}}_c\rangle = \int \dot{\mathbf{r}}_c\psi d\mathbf{q}. \tag{5}$$

At steady state, the distribution of the end-to-end vector is given by

$$n\frac{\partial}{\partial \mathbf{q}}\cdot(\dot{\mathbf{q}}\psi) = -\frac{\partial}{\partial \mathbf{r}_c}\cdot(n\dot{\mathbf{r}}_c\psi). \tag{6}$$

Approximating $\dot{\mathbf{r}}_c\psi$ by $\langle\dot{\mathbf{r}}_c\rangle$ in Eq. (6) and making use of Eq. (4) gives

$$\frac{\partial}{\partial \mathbf{q}}\cdot(\dot{\mathbf{q}}\psi) = 0. \tag{7}$$

After determining ψ from Eq. (7), Eq. (4) is solved for the center-of-mass distribution. In principle, computing successive approximations to the right-hand side of Eq. (6) would improve the solutions of ψ and n. However, the orientation distribution function equilibrates much faster than the polymer migrates and diffuses across streamlines, so the approximation made in Eq. (7) is not severe.[7] Additionally, comparing the results of the theory with simulations (Sec. III) demonstrates that errors associated with this assumption are quantitative, rather that qualitative.

A. Velocity expressions

The polymer is confined between two planar walls, positioned at $y=0$ and $y=h$, and moves under the combined action of a pressure driven flow (in the x-direction) and an external force, $\mathbf{F}_1^E=\mathbf{F}_2^E=F^E\mathbf{e}_x$, where F^E is the magnitude of the force and $\mathbf{e}_x$ is a unit vector parallel to the flow direction. The external force acts only on the beads, and on each bead with the same forcing; the additional effects of electrostatic forces and counter ions, necessary to address electrophoresis of polyelectrolytes, are considered in Sec. IV. In addition to the external force, an intramolecular force, $\mathbf{F}^S=\mathbf{F}_1^S=-\mathbf{F}_2^S$, acts in the opposite direction on each bead.

In the absence of inertia, the velocity of each bead (i) is determined from the force balance

$$\mathbf{F}_i^H + \mathbf{F}_i^B + \mathbf{F}_i^S + \mathbf{F}_i^E = 0, \tag{8}$$

where $\mathbf{F}_i^H$ is the viscous drag and the Brownian force is

$$\mathbf{F}_i^B = -k_BT\frac{\partial}{\partial \mathbf{r}_i}\ln\Psi. \tag{9}$$

Implicit in the expression for the Brownian force is an instantaneous average over the solvent degrees of freedom.

The hydrodynamic force on each bead is proportional to the difference in velocity of the bead, $\dot{\mathbf{r}}_i$, and the fluid velocity evaluated at the bead center,

$$\mathbf{F}_i^H = -\xi[\dot{\mathbf{r}}_i - (\mathbf{v}_0(\mathbf{r}_i) + \mathbf{v}'(\mathbf{r}_i))], \tag{10}$$

where $\xi=6\pi\eta a$ is the Stokes resistance of a bead with hydrodynamic radius a within a fluid of viscosity η. The quadratic flow field, $\mathbf{v}_0$, is due to the pressure gradient. The velocity disturbance, $\mathbf{v}'$, results from the fluid motion generated by the forces applied to the other bead.

In an infinite medium, the velocity field at a point $\mathbf{r}$ created by a point force located at the origin is related through the Oseen tensor,

$$\mathbf{S}(\mathbf{r}) = \frac{1}{8\pi\eta|\mathbf{r}|}\left(\mathbf{I} + \frac{\mathbf{rr}}{|\mathbf{r}|^2}\right), \tag{11}$$

where $\mathbf{I}$ is the identity matrix and $|\mathbf{r}|$ indicates the magnitude of $\mathbf{r}$. However, the velocity disturbance must include the effect of the bounding walls to capture all of the mechanisms governing the migration of the dumbbell. Here, the method of reflections[16,17] is used to calculate the additional flow field arising from cancellation of the source velocity [Eq. (11)] along the boundary surfaces. The combined effect of two boundaries is approximated by superposing the canceling flow fields from each surface.[7] Numerical evidence[3,4] suggests that this approximation is reasonable when the separation between the walls is an order of magnitude larger than

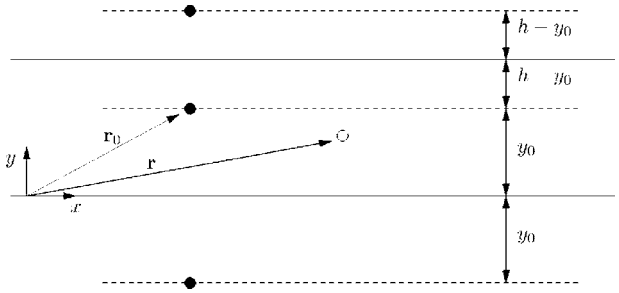

FIG. 1. The geometry used in calculating the disturbance velocity at $\mathbf{r}$ caused by a point force at $\mathbf{r}_0$. The calculation includes the first image sources at $\mathbf{r}_0+2(h-y_0)\mathbf{e}_y$ and $\mathbf{r}_0-2y_0\mathbf{e}_y$ which cancel the normal velocity of the source at the top and bottom walls. Additional force dipoles and stress doublets are needed to cancel the tangential velocities at the walls.

the radius of gyration of the polymer. The disturbance velocity at a position $\mathbf{r}$ due to a point force located at $\mathbf{r}_0$ is[18]

$$\mathbf{v}'(\mathbf{r}) = -(\mathbf{S}(\mathbf{r}-\mathbf{r}_0)+\mathbf{G}(\mathbf{r},\mathbf{r}_0))\cdot\mathbf{F}^H, \tag{12}$$

where $\mathbf{F}^H=-(\mathbf{F}^B+\mathbf{F}^S+\mathbf{F}^E)$ is the sum of all nonhydrodynamic forces at $\mathbf{r}_0$ and the hydrodynamic interaction tensor $\mathbf{G}$ is

$$\begin{aligned}\mathbf{G}(\mathbf{r},\mathbf{r}_0) = &-\mathbf{S}(\mathbf{r}-\mathbf{r}_0+2y_0\mathbf{e}_y)-\mathbf{S}(\mathbf{r}-\mathbf{r}_0-2(h-y_0)\mathbf{e}_y)\\ &-2y_0\mathbf{S}^D(\mathbf{r}-\mathbf{r}_0+2y_0\mathbf{e}_y)\\ &-2(y_0-h)\mathbf{S}^D(\mathbf{r}-\mathbf{r}_0-2(h-y_0)\mathbf{e}_y)\\ &+2y_0^2\mathbf{P}^D(\mathbf{r}-\mathbf{r}_0+2y_0\mathbf{e}_y)\\ &+2(y_0-h)^2\mathbf{P}^D(\mathbf{r}-\mathbf{r}_0-2(h-y_0)\mathbf{e}_y).\end{aligned} \tag{13}$$

The geometry is illustrated in Fig. 1; y_0 is the distance of the source point from the boundary at $y=0$. The two contributions of the Oseen tensor within $\mathbf{G}$ are due to images of the Stokeslet above the top wall and below the bottom wall. The potential dipoles, $\mathbf{P}^D$, and Stokeslet doublets, $\mathbf{S}^D$, are included to enforce the tangential no-slip conditions on the top and bottom walls, with

$$\mathbf{P}^D(\mathbf{r}) = \frac{1}{8\pi\eta|\mathbf{r}|^5}\begin{vmatrix}|\mathbf{r}|^2-3r_x^2 & 3r_xr_y & -3r_xr_z\\ -3r_yr_x & -|\mathbf{r}|^2+3r_y^2 & -3r_yr_z\\ -3r_zr_x & 3r_zr_y & |\mathbf{r}|^2-3r_z^2\end{vmatrix}, \tag{14}$$

$$\mathbf{S}^D(\mathbf{r}) = r_y\mathbf{P}^D(\mathbf{r})+\frac{1}{8\pi\eta|\mathbf{r}|^3}\begin{vmatrix}0 & -r_x & 0\\ -r_x & 0 & -r_z\\ 0 & -r_z & 0\end{vmatrix}. \tag{15}$$

The velocities of the beads are determined from Eqs. (8), (10), and (12),

$$\dot{\mathbf{r}}_i = \mathbf{v}_0(\mathbf{r}_i)+\sum_{j=1}^{2}\left(\mathbf{\Omega}_{ij}+\frac{\delta_{ij}}{\xi}\mathbf{I}\right)\cdot(\mathbf{F}_j^B+\mathbf{F}_j^S+\mathbf{F}_j^E), \tag{16}$$

where δ_{ij} is the Kronecker delta and the hydrodynamic interaction matrix is

$$\mathbf{\Omega}_{ij} = \begin{cases}\mathbf{G}(\mathbf{r}_i,\mathbf{r}_i) & \text{if } i=j,\\ \mathbf{S}(\mathbf{r}_i-\mathbf{r}_j)+\mathbf{G}(\mathbf{r}_i,\mathbf{r}_j) & \text{if } i\neq j.\end{cases} \tag{17}$$

Note that the self-interaction, $\mathbf{\Omega}_{ii}$, does not include the mobility of the isolated bead, but only the hydrodynamic effect of the walls, $\mathbf{G}(\mathbf{r}_i,\mathbf{r}_i)$.

The velocity of the center-of-mass of the dumbbell, $\dot{\mathbf{r}}_c=(\dot{\mathbf{r}}_1+\dot{\mathbf{r}}_2)/2$, and rate of change of the connector vector, $\dot{\mathbf{q}}=\dot{\mathbf{r}}_2-\dot{\mathbf{r}}_1$, are evaluated from Eq. (16),

$$\begin{aligned}\dot{\mathbf{r}}_c = &\mathbf{v}_0(\mathbf{r}_c)+\frac{1}{8}\mathbf{qq}:\nabla\nabla\mathbf{v}_0+\frac{1}{2}\bar{\mathbf{\Omega}}\cdot\mathbf{F}^S+\frac{2}{k_BT}\mathbf{D}_K\cdot\mathbf{F}^E\\ &+\frac{k_BT}{2}\bar{\mathbf{\Omega}}\cdot\frac{\partial\ln(\Psi)}{\partial\mathbf{q}}-\mathbf{D}_K\cdot\frac{\partial\ln(\Psi)}{\partial\mathbf{r}_c},\end{aligned} \tag{18}$$

$$\begin{aligned}\dot{\mathbf{q}} = &\mathbf{q}\cdot\nabla\mathbf{v}_0-\left(\frac{2}{\xi}\mathbf{I}+\hat{\mathbf{\Omega}}\right)\cdot\mathbf{F}^S-\bar{\bar{\mathbf{\Omega}}}\cdot\mathbf{F}^E\\ &-k_BT\left(\frac{2}{\xi}\mathbf{I}+\hat{\mathbf{\Omega}}\right)\cdot\frac{\partial\ln(\Psi)}{\partial\mathbf{q}}+\frac{k_BT}{2}\bar{\bar{\mathbf{\Omega}}}\cdot\frac{\partial\ln(\Psi)}{\partial\mathbf{r}_c},\end{aligned} \tag{19}$$

where the motion of the dumbbell due to the imposed velocity, $\mathbf{v}_0$, at the points $\mathbf{r}_1$ and $\mathbf{r}_2$ has been approximated by a second-order Taylor expansion about the center-of-mass, $\mathbf{r}_c$. The hydrodynamic interaction tensors appearing in Eqs. (18) and (19) are linear combinations of $\mathbf{\Omega}_{ij}$,

$$\mathbf{D}_K = \frac{k_BT}{4}\left[\frac{2}{\xi}\mathbf{I}+\mathbf{\Omega}_{11}+\mathbf{\Omega}_{22}+\mathbf{\Omega}_{21}+\mathbf{\Omega}_{12}\right], \tag{20}$$

$$\bar{\mathbf{\Omega}} = (\mathbf{\Omega}_{11}-\mathbf{\Omega}_{22})+(\mathbf{\Omega}_{21}-\mathbf{\Omega}_{12}), \tag{21}$$

$$\hat{\mathbf{\Omega}} = (\mathbf{\Omega}_{11}+\mathbf{\Omega}_{22})-(\mathbf{\Omega}_{12}+\mathbf{\Omega}_{21}), \tag{22}$$

$$\bar{\bar{\mathbf{\Omega}}} = (\mathbf{\Omega}_{11}-\mathbf{\Omega}_{22})+(\mathbf{\Omega}_{12}-\mathbf{\Omega}_{21}). \tag{23}$$

The analysis is simplified by considering only those situations where the polymer is far from the wall in comparison to its end-to-end distance. As derived in the Appendix, the explicit result of expanding about $\mathbf{r}_c$ to linear order in $\mathbf{q}$ is

$$\mathbf{D}_K = \frac{k_BT}{2\xi}[\mathbf{I}+\xi\mathbf{S}(\mathbf{q})-\omega(y_c)(\mathbf{I}+\mathbf{e}_y\mathbf{e}_y)], \tag{24}$$

$$\bar{\mathbf{\Omega}} = \lambda(y_c)\begin{vmatrix}-q_y & -q_x & 0\\ q_x & -2q_y & q_z\\ 0 & -q_z & -q_y\end{vmatrix}, \tag{25}$$

$$\hat{\mathbf{\Omega}} = -2\mathbf{S}(\mathbf{q}), \tag{26}$$

$$\bar{\bar{\mathbf{\Omega}}} = \lambda(y_c)\begin{vmatrix}-q_y & q_x & 0\\ -q_x & -2q_y & -q_z\\ 0 & q_z & -q_y\end{vmatrix}, \tag{27}$$

where the scalar functions $\lambda(y_c)$ and $\omega(y_c)$ depend only on the position of the center-of-mass in the channel,

$$\lambda(y_c) = \frac{3}{32\pi\eta}\left(\frac{1}{y_c^2}-\frac{1}{(y_c-h)^2}\right), \tag{28}$$

$$\omega(y_c) = \frac{9a}{8}\left(\frac{1}{y_c} - \frac{1}{y_c - h}\right). \tag{29}$$

B. Probability distribution

Substituting Eq. (18) into Eq. (5) and multiplying by n gives the flux of the center-of-mass,

$$n\langle \dot{\mathbf{r}}_c\rangle = n\mathbf{v}_0 + \frac{n}{8}\langle \mathbf{qq}\rangle : \nabla\nabla \mathbf{v}_0 + \frac{n}{2}\langle \bar{\mathbf{\Omega}} \cdot \mathbf{F}^S\rangle + \frac{2n}{k_BT}\langle \mathbf{D}_K \cdot \mathbf{F}^E\rangle + \frac{nk_BT}{2}\left\langle \bar{\mathbf{\Omega}} \cdot \frac{\partial \ln \psi}{\partial \mathbf{q}}\right\rangle - \langle \mathbf{D}_K\rangle \cdot \frac{\partial n}{\partial \mathbf{r}_c} - n\left\langle \mathbf{D}_K \cdot \frac{\partial \ln \psi}{\partial \mathbf{r}_c}\right\rangle, \tag{30}$$

which matches the expression in Eq. (28) of Ma and Graham[7] with an additional contribution associated with the external force, $\mathbf{F}^E$. For steady flow, the flux normal to the bounding walls ($n\langle \dot{\mathbf{r}}_c\rangle \cdot \mathbf{e}_y$) is zero,

$$n\langle \dot{\mathbf{r}}_c\rangle \cdot \mathbf{e}_y = 0 = \frac{\lambda}{2} nH\langle q_x^2 - 2q_y^2 + q_z^2\rangle + nF^E\langle S_{yx}\rangle - \frac{nk_BT}{2}\frac{\partial}{\partial y_c}\langle S_{yy}\rangle - \frac{k_BT}{2\xi}[1 + \xi\langle S_{yy}\rangle - 2\omega(y_c)]\frac{\partial n}{\partial y_c}. \tag{31}$$

The expansions for the interaction tensors [Eqs. (25)–(27)] have been substituted into Eq. (30) together with a linear spring force, $\mathbf{F}^S = H\mathbf{q}$, to give Eq. (31).

Calculating the distribution across the channel, $n(y_c)$, requires the ensemble averages over $\mathbf{q}$ that appear in Eq. (31). The approximation of Eq. (7) is used to determine ψ and then calculate the ensemble averages. Using Eq. (19) in Eq. (7) gives

$$0 = \frac{\partial}{\partial \mathbf{q}} \cdot \left[\mathbf{q} \cdot \nabla \mathbf{v}_0 \psi - \left(\frac{2}{\xi}\mathbf{I} + \hat{\mathbf{\Omega}}\right) \cdot \mathbf{F}^S \psi - k_BT\left(\frac{2}{\xi}\mathbf{I} + \hat{\mathbf{\Omega}}\right) \cdot \frac{\partial \psi}{\partial \mathbf{q}} - \bar{\bar{\mathbf{\Omega}}} \cdot \mathbf{F}^E \psi + \frac{k_BT}{2}\bar{\bar{\mathbf{\Omega}}} \cdot \frac{\partial \ln(\Psi)}{\partial \mathbf{r}_c}\psi\right]. \tag{32}$$

In recent work,[7,19] authors have ignored the influence of hydrodynamic interactions on the orientation distribution, ψ, used a FENE-P spring force, and then solved numerically for the deformation tensor, $\langle \mathbf{qq}\rangle$, as a function of the transverse position (y_c) within the channel. Once determined, the components of the deformation tensor were used to evaluate the quantities necessary for calculating $n(y_c)$.

In the present circumstances, hydrodynamic interactions must be retained within Eq. (32) to predict migration due to the external force. Specifically, the term $\bar{\bar{\mathbf{\Omega}}} \cdot \mathbf{F}^E$ which results from the interaction with the bounding walls must be included, though the other contributions proportional to $\bar{\bar{\mathbf{\Omega}}}$ and $\hat{\mathbf{\Omega}}$ are still neglected. A linear spring force is used instead of the FENE-P spring force and simplifying Eq. (32), using Eq. (27) for $\bar{\bar{\mathbf{\Omega}}}$, gives

$$0 = \dot{\gamma} q_y \frac{\partial \psi}{\partial q_x} - \frac{2H}{\xi}\left(3\psi + \mathbf{q} \cdot \frac{\partial \psi}{\partial \mathbf{q}}\right) - \frac{2k_BT}{\xi}\frac{\partial^2 \psi}{\partial \mathbf{q}^2} + (\lambda F^E)\left(q_y \frac{\partial \psi}{\partial q_x} + q_x \frac{\partial \psi}{\partial q_y}\right). \tag{33}$$

In plane Poiseuille flow, $\dot{\gamma}$ is position dependent,

$$\dot{\gamma} = 2\bar{\dot{\gamma}}\left(1 - \frac{2}{h}y_c\right), \tag{34}$$

where the mean shear rate is $\bar{\dot{\gamma}}$.

A length $\sqrt{k_BT/H}$ is defined to make the end-to-end vector dimensionless,

$$\mathbf{q}^* = \sqrt{\frac{H}{k_BT}}\mathbf{q}, \tag{35}$$

and dimensionless values for the shear rate and forces are introduced,

$$\dot{\gamma}^* = \frac{\xi}{H}\dot{\gamma}, \tag{36}$$

$$F^* = \frac{\xi}{\eta k_BT}F^E, \tag{37}$$

$$\lambda^* = \frac{\eta k_BT}{H}\lambda. \tag{38}$$

In terms of these parameters, the explicit solution of Eq. (33) is

$$\psi(y, \mathbf{q}) = \frac{1}{J}\exp\left[-\frac{1}{2c_4}(c_1(q_x^*)^2 + c_2 q_x^* q_y^* + c_3(q_y^*)^2 + c_4(q_z^*)^2)\right], \tag{39}$$

with coefficients

$$c_1 = 1 - \tfrac{1}{8}(\lambda^* F^*)\dot{\gamma}^*, \tag{40}$$

$$c_2 = -(\lambda^* F^*) - \tfrac{1}{2}\dot{\gamma}^*, \tag{41}$$

$$c_3 = 1 + \tfrac{1}{8}[(\dot{\gamma}^*)^2 + (\lambda^* F^*)\dot{\gamma}^*], \tag{42}$$

$$c_4 = 1 + \tfrac{1}{16}(\dot{\gamma}^*)^2, \tag{43}$$

and normalization

$$J = \left[\frac{2\pi k_BT}{H}\right]^{3/2}\left[\frac{4c_4^2}{4c_1c_3 - c_2^2}\right]^{1/2}. \tag{44}$$

The value of $\langle q_x^2 - 2q_y^2 + q_z^2\rangle$ can be calculated using Eq. (39),

$$\langle q_x^2 - 2q_y^2 + q_z^2\rangle = \left(\frac{k_BT}{H}\right)\frac{(\dot{\gamma}^*)^2 + (\lambda^* F^*)\dot{\gamma}^* - 2(\lambda^* F^*)^2}{8 - 2[(\lambda^* F^*)\dot{\gamma}^* + (\lambda^* F^*)^2]}. \tag{45}$$

However, calculating $\langle S_{yx}\rangle$ and $\langle S_{yy}\rangle$ is problematic.[15] For the conditions of interest, terms proportional to $\dot{\gamma}^*$ and $\lambda^* F^*$ are of order one or smaller over most of the channel width which is accessible to the polymer. The values are in fact zero at the

centerline and the polymer cannot access positions near the wall due to excluded volume. Consequently, Eq. (39) is expanded about $\dot{\gamma}^*=0$ and $\lambda^* F^*=0$, and to second order,

$$\psi(y,\mathbf{q}) = \psi_{\mathrm{eq}}\Bigg[1+\frac{1}{2}\left(\frac{1}{2}\dot{\gamma}^*+\lambda^* F^*\right)q_x^* q_y^* + \frac{1}{32}(\dot{\gamma}^*)^2(-1-(q_y^*)^2+(q_x^*)^2+(q_x^* q_y^*)^2) + \frac{1}{16}\dot{\gamma}^*(\lambda^* F^*)(-2-(q_y^*)^2+(q_x^*)^2+2(q_x^* q_y^*)^2) + \frac{1}{8}(\lambda^* F^*)^2(-1+(q_x^* q_y^*)^2)\Bigg], \tag{46}$$

where the equilibrium distribution for the dumbbell is

$$\psi_{\mathrm{eq}} = \left(\frac{H}{2\pi k_B T}\right)^{3/2}\exp\left(-\frac{1}{2}((q_x^*)^2+(q_y^*)^2+(q_z^*)^2)\right). \tag{47}$$

Note that this same result can be derived by constructing a perturbation solution for ψ around $\dot{\gamma}^*=0$ and $\lambda^* F^*=0$, in the same manner as done for a simple shear flow,[15,20] and then solving Eq. (32) for the 0th, 1st, and 2nd order solutions; this procedure could be followed for a variety of nonlinear dumbbell models.

Equation (46) can now be used to calculate $\langle S_{yx}\rangle$ and $\langle S_{yy}\rangle$,

$$\langle S_{yx}\rangle = \left(\frac{1}{\eta}\sqrt{\frac{H}{k_B T}}\right)\frac{1}{60(2\pi)^{3/2}}[\dot{\gamma}^*+2(\lambda^* F^*)], \tag{48}$$

$$\langle S_{yy}\rangle = \left(\frac{1}{\eta}\sqrt{\frac{H}{k_B T}}\right)\frac{1}{840(2\pi)^{3/2}}[560-11(\dot{\gamma}^*)^2-3(\lambda^* F^*)^2 - 37\dot{\gamma}^*(\lambda^* F^*)]. \tag{49}$$

In addition, $\langle q_x^2-2q_y^2+q_z^2\rangle$ is recalculated using Eq. (46),

$$\langle q_x^2-2q_y^2+q_z^2\rangle = \left(\frac{k_B T}{H}\right)\frac{1}{8}[(\dot{\gamma}^*)^2+(\lambda^* F^*)\dot{\gamma}^*-2(\lambda^* F^*)^2]; \tag{50}$$

this approximation can be compared to the exact expression in Eq. (45).

C. Center of mass distribution

Using the ensemble averages from Eqs. (48)–(50) within Eq. (31) and setting the flux in the transverse (y) direction to zero gives a differential equation for the probability distribution of the center-of-mass across the channel,

$$\mathcal{D}^*\frac{\partial \ln[n(y^*)]}{\partial y^*} = \mathcal{S}^*+\mathcal{F}^*+\mathcal{G}^*, \tag{51}$$

where the values of $\mathcal{D}^*$, $\mathcal{S}^*$, $\mathcal{F}^*$, and $\mathcal{G}^*$ are given by

$$\mathcal{D}^* = 1+\frac{a^*}{280\sqrt{2\pi}}[560-11(\dot{\gamma}^*)^2-3(\lambda^* F^*)^2 - 37\dot{\gamma}^*(\lambda^* F^*)]-\frac{9a^* h^*}{4y^*(y^*-h^*)}, \tag{52}$$

$$\mathcal{S}^* = \frac{3\pi}{4}a^*\lambda^*[(\dot{\gamma}^*)^2+(\lambda^* F^*)\dot{\gamma}^*-2(\lambda^* F^*)^2], \tag{53}$$

$$\mathcal{F}^* = \frac{1}{30(2\pi)^{3/2}}F^*[\dot{\gamma}^*+2(\lambda^* F^*)], \tag{54}$$

$$\mathcal{G}^* = \frac{1}{280\sqrt{2\pi}}a^*\frac{\partial}{\partial y^*}[11(\dot{\gamma}^*)^2+3(\lambda^* F^*)^2+37\dot{\gamma}^*(\lambda^* F^*)]. \tag{55}$$

The position y_c, height h, and radius a have been scaled by the length $\sqrt{k_B T/H}$ to give y^*, h^*, and a^*. The diffusivity in the transverse direction, $\mathcal{D}^*$, has been normalized by the diffusivity of the freely draining dumbbell, $D_0=k_B T/2\xi$. The term $\mathcal{S}^*$ is related to the stress component $(\lambda H\langle q_x^2-2q_y^2+q_z^2\rangle/2)$, while $\mathcal{F}^*$ describes the migration of an oriented dumbbell in an external force. The preferential orientation arises both from the local shear rate and, near the wall, from the orientation induced by the external force itself. An additional flux arising from the gradient in the diffusivity is contained within $\mathcal{G}^*$.

To enable direct comparison with simulations,[4,8] two different Peclet numbers have been defined. One comes from the ratio of the mean shear rate to the diffusivity of the freely draining dumbbell,

$$\mathrm{Pe}_f = \frac{\bar{\dot{\gamma}}R_g^2}{D_0} = \frac{3\xi\bar{\dot{\gamma}}}{2H}, \tag{56}$$

where R_g is the radius of gyration,

$$R_g = \sqrt{\frac{3k_B T}{4H}}. \tag{57}$$

The other Peclet number is due to the external force acting on the polymer,

$$\mathrm{Pe} = \frac{R_g u_p}{D_0} = \left(\frac{3}{k_B T H}\right)^{1/2}F^E, \tag{58}$$

where u_p is the velocity of the free draining polymer. All lengths have been nondimensionalized by the radius of gyration,

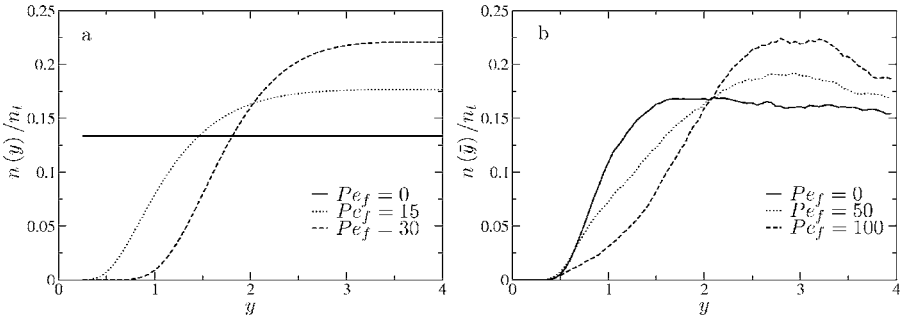

FIG. 2. Distribution of the center-of-mass for pressure-driven flow only. (a) Results from the theory neglecting gradients in the diffusivity. (b) Results of numerical simulations reported by Usta *et al.* (Ref. 4). Results are plotted between the bounding wall at $\bar{y}=0$ and centerline ($\bar{y}=4$) of the channel.

$$\bar{y} = \frac{y_c}{R_g},$$

$$\bar{a} = \frac{a}{R_g}, \tag{59}$$

$$\bar{h} = \frac{h}{R_g}.$$

Rewriting Eq. (51) using the definitions in Eqs. (56)–(59) gives

$$\bar{\mathcal{D}}\frac{\partial \ln[n(\bar{y})]}{\partial \bar{y}} = \bar{\mathcal{S}} + \bar{\mathcal{F}} + \bar{\mathcal{G}}, \tag{60}$$

where

$$\bar{\mathcal{D}} = 1 + \sqrt{\frac{3\bar{a}^2}{2\pi}}\left[1 - \frac{11}{315\bar{h}^2}\mathrm{Pe}_f^2(2\bar{y}-\bar{h})^2 - \frac{27\bar{a}^2\bar{h}^2}{35840}\mathrm{Pe}^2\frac{(2\bar{y}-\bar{h})^2}{\bar{y}^4(\bar{y}-\bar{h})^4} \mp \frac{37\bar{a}}{1120}\mathrm{Pe}\,\mathrm{Pe}_f\frac{(2\bar{y}-\bar{h})^2}{\bar{y}^2(\bar{y}-\bar{h})^2}\right] - \frac{9\bar{a}\bar{h}}{4}\frac{1}{\bar{y}(\bar{y}-\bar{h})}, \tag{61}$$

$$\bar{\mathcal{S}} = -\frac{\bar{a}}{8\bar{h}}\mathrm{Pe}_f^2\frac{(2\bar{y}-\bar{h})^3}{\bar{y}^2(\bar{y}-\bar{h})^2} \mp \frac{9\bar{a}^2\bar{h}}{256}\mathrm{Pe}_f\,\mathrm{Pe}\frac{(2\bar{y}-\bar{h})^3}{\bar{y}^4(\bar{y}-\bar{h})^4} + \frac{81\bar{a}^3\bar{h}^3}{4096}\mathrm{Pe}^2\frac{(2\bar{y}-\bar{h})^3}{\bar{y}^6(\bar{y}-\bar{h})^6}, \tag{62}$$

$$\bar{\mathcal{F}} = \mp\frac{\sqrt{6}\bar{a}}{60\sqrt{\pi}\bar{h}}\mathrm{Pe}_f\,\mathrm{Pe}(2\bar{y}-\bar{h}) - \frac{3\sqrt{6}\bar{a}^2\bar{h}}{320\sqrt{\pi}}\mathrm{Pe}^2\frac{2\bar{y}-\bar{h}}{\bar{y}^2(\bar{y}-\bar{h})^2}, \tag{63}$$

$$\bar{\mathcal{G}} = \sqrt{\frac{3\bar{a}^2}{2\pi}}\left[\frac{44}{315\bar{h}^2}\mathrm{Pe}_f^2(2\bar{y}-\bar{h}) + \frac{27\bar{a}^2\bar{h}^2}{8960}\mathrm{Pe}^2\frac{(2\bar{y}-\bar{h})(3\bar{y}^2-3\bar{y}\bar{h}+\bar{h}^2)}{\bar{y}^5(\bar{h}-\bar{y})^5} \mp \frac{37\bar{a}}{560}\mathrm{Pe}_f\,\mathrm{Pe}\frac{(2\bar{y}-\bar{h})(2\bar{y}^2-2\bar{y}\bar{h}+\bar{h}^2)}{\bar{y}^3(\bar{y}-\bar{h})^3}\right]. \tag{64}$$

For terms having a sign of $\mp$, the minus sign corresponds to the case where the external force acts in the same direction of the flow field ($F^E>0$) and the plus sign to an external force opposing the flow field ($F^E<0$). Note that the functional dependence on the positions is explicit in Eqs. (60)–(64), in contrast to Eqs. (51)–(55) which present the results in terms of the local values of the shear rate and external force.

III. RESULTS AND DISCUSSION

The time independent distribution of the polymer was determined from Eq. (60) for the cases of flow only, force only, and combinations of force and flow. The height of the channel in comparison to the radius of gyration, $\bar{h}$, was set to eight and the hydrodynamic radius, $\bar{a}$, to 0.125 for all results shown. These same parameters were used in the numerical simulations of multibead chains,[4,8] which are compared here with the results of the theory.

Terms within $\bar{\mathcal{S}}$ and $\bar{\mathcal{G}}$ proportional to $\bar{a}^3$ were ignored. These terms negligibly impact the distribution in the bulk of the channel, though very near the wall these terms dominate. However, a force to maintain the excluded volume of the polymer in the vicinity of the wall was not included in the force balance of Eq. (8). Consequently, the concentration near the wall was set to zero by performing the integration of Eq. (60) between $y=0.25R_g$ and $y=h-0.25R_g$, rather than 0 and h. The distribution $n(\bar{y})$ was normalized by n_t, where

$$n_t = \int_{\bar{y}=0.25}^{\bar{h}-0.25} n(\bar{y})d\bar{y}. \tag{65}$$

As a final simplification, the diffusivity, $\bar{\mathcal{D}}$, was set to unity in all reported results. Full evaluation of $\bar{\mathcal{D}}$ leads to negative values for center-of-mass positions near the wall due to the use of the approximate interaction tensors. The diffusivity was regularized in some studies (not presented here) by resetting negative values of $\bar{\mathcal{D}}$ to a small positive value. In all cases, the effect was a small shift of the distribution towards the center of the channel as compared to the results presented here with $\bar{\mathcal{D}}=1$.

A. Pressure-driven flow

For a pressure driven flow where the gradient terms are ignored ($\bar{\mathcal{G}}=0$), Eq. (60) reduces to

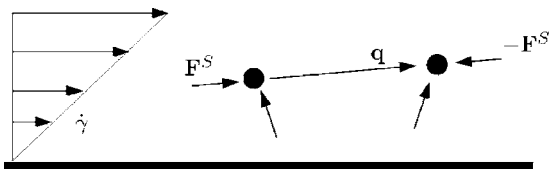

FIG. 3. Mechanism for migration away from the wall due to shear flow. The flow field aligns and stretches the dumbbell. The spring force, which is in tension, generates a disturbance flow and a net velocity away from the no-slip boundary.

$$\frac{\partial \ln[n(\bar{y})]}{\partial \bar{y}} = -\frac{\bar{a}}{8\bar{h}}\mathrm{Pe}_f^2 \frac{(2\bar{y}-\bar{h})^3}{\bar{y}^2(\bar{y}-\bar{h})^2}. \tag{66}$$

The solution of this equation,

$$\frac{n(\bar{y})}{n_t} = \exp\left[-\frac{\bar{a}\,\mathrm{Pe}_f^2}{2}\left(\frac{1}{4\bar{y}} + \frac{\ln \bar{y}}{\bar{h}} + \frac{1}{4(\bar{h}-\bar{y})} + \frac{\ln(\bar{h}-\bar{y})}{\bar{h}}\right)\right], \tag{67}$$

predicts a depletion layer near the boundaries which increases with Pe_f, as seen in Fig. 2(a). The depletion layer results from the hydrodynamic interaction of the dumbbell with the wall, as previously identified.[2,7] As illustrated in Fig. 3, a strong shear flow tends to orient the connector vector $\mathbf{q}$ such that the polymer is in tension. The tension in the spring creates a force $\mathbf{F}^S$ acting on each bead and a consequent velocity disturbance on the other bead. Due to the break in symmetry caused by the presence of the wall, the velocity disturbance results in a net lift of the center-of-mass away from the boundary.

The results in Fig. 2(a) differ from the results of numerical simulations[2,4] in two qualitative aspects. First, simulation results exhibited a significant depletion near the walls at equilibrium which was not observed in the analytical results due to the absence of an excluded volume force with the wall. Secondly, in the simulations the maximum in $n(\bar{y})$ occurs off-center [see Fig. 2(b)], implying the existence of a secondary mechanism promoting migration towards the boundaries in competition with the shear-induced migration (Fig. 3). This additional mechanism arises from the variation in diffusivity of the polymer caused by the nonuniform shear flow.[21] The transverse diffusivity of a polymer near the center of the channel, where the shear rate approaches zero, is higher than a polymer near the wall that is highly extended

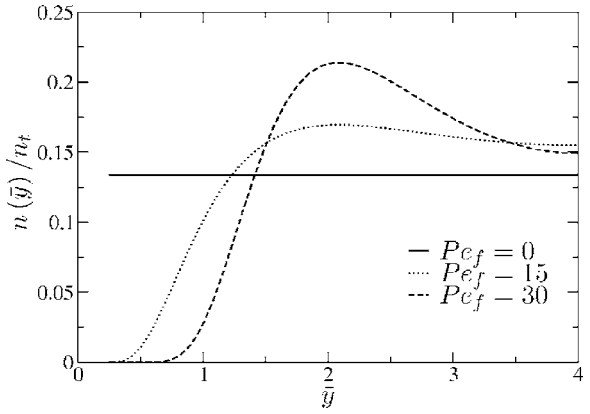

FIG. 4. Distribution of the center-of-mass for pressure-driven flow only. Theoretical results including the gradient in the diffusivity.

by the shear; the gradient in transverse diffusivity results in a drift of the polymer away from the centerline. This effect is captured by the theory within the gradient ($\bar{\mathcal{G}}$) terms. Including these terms with those in Eq. (66) and integrating gives

$$\frac{n(\bar{y})}{n_t} = \exp\left[-\frac{\bar{a}\,\mathrm{Pe}_f^2}{2}\left(\frac{1}{4\bar{y}} + \frac{\ln \bar{y}}{\bar{h}} + \frac{1}{4(\bar{h}-\bar{y})} + \frac{\ln(\bar{h}-\bar{y})}{\bar{h}} + \sqrt{\frac{3}{2\pi}}\frac{88}{315\bar{h}^2}\bar{y}(\bar{y}-\bar{h})\right)\right]. \tag{68}$$

Plots of this solution in Fig. 4 demonstrate that the gradient in diffusivity moves the maximum in $n(\bar{y})$ away from the centerline and towards the boundary.

Quantitative differences between the numerical and analytical solutions are apparent in Fig. 2. Predicting a similar depletion layer near the wall requires a value of Pe_f which is approximately one third of the value used in the simulations. Note that the highest value of $\mathrm{Pe}_f=30$ corresponds to $\dot{\gamma}^*=20$ when evaluated at $\bar{y}=2$. This value may be too large for the expansion in Eq. (46), which assumes $\dot{\gamma}^*$ is of order one or less. However, the theory contains no adjustable parameters and is yet able to capture the essence of the simulation results.

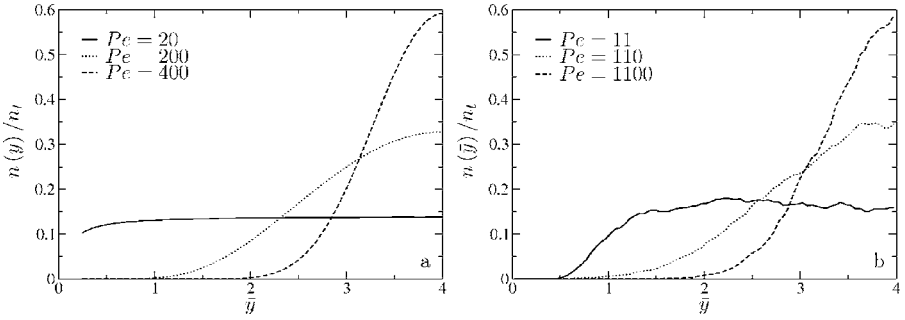

FIG. 5. Distribution of center-of-mass for an external force when there is no imposed flow field ($\mathrm{Pe}_f=0$). (a) Results from the theory and (b) results from numerical simulations by Usta *et al.* (Ref. 8) are shown.

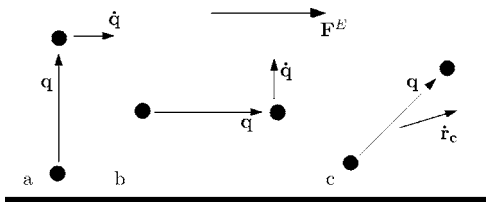

FIG. 6. Mechanism for migration away from the wall due to an external force $\mathbf{F}^E$. The external force rotates a dumbbell to an orientation which results in a drift away from the wall, as shown in (c). For example, a dumbbell perpendicular to the wall (a) rotates towards alignment with the wall, whereas a dumbbell parallel with the wall (b) rotates away from the wall.

B. Migration due to an external force

In the absence of a flow field, Eq. (60) reduces to

$$\frac{\partial \ln[n(\bar{y})]}{\partial \bar{y}} = -\frac{3\sqrt{6}\bar{a}^2\bar{h}}{320\sqrt{\pi}}\mathrm{Pe}^2\frac{2\bar{y}-\bar{h}}{\bar{y}^2(\bar{y}-\bar{h})^2}, \tag{69}$$

where terms of order $\bar{a}^3$ have been neglected. Integrating gives an explicit expression for the distribution across the channel,

$$\frac{n(\bar{y})}{n_t} = \exp\left[-\frac{3\sqrt{6}\bar{a}^2\bar{h}}{320\sqrt{\pi}}\mathrm{Pe}^2\frac{1}{\bar{y}(\bar{h}-\bar{y})}\right]. \tag{70}$$

The external force, if sufficiently large compared to the thermal fluctuations, results in a strong migration of the polymer away from the wall as seen in Fig. 5(a).

The migration arises from the rotation of the dumbbell near the wall to an average orientation centered about the 45° line, which results in a drift away from the wall under the action of an external force as illustrated in Fig. 6. The first step of the process, the rotation, occurs directly as a result of the hydrodynamic interaction with the wall; the term $-\overline{\overline{\mathbf{\Omega}}}\cdot\mathbf{F}^E$ appearing in Eq. (19) is responsible for the rotation, but $\overline{\overline{\mathbf{\Omega}}}$ is zero if the wall is not present. Whether aligned perpendicular or parallel to the wall, the polymer rotates towards the preferred orientation shown in Fig. 6. The oriented dumbbell then couples with the external force through the hydrodynamic interaction between the beads to move the polymer away from the wall.

The analytical result at Pe=200 compares well with the simulation performed for Pe=110, suggesting a difference of approximately 2 in the effective Peclet numbers. At the highest Peclet number, Pe=400, $\lambda^* F^*$ is approximately 4 at $\bar{y}=2$, which may still be within the radius of convergence of the Taylor expansion since the coefficients in Eq. (46) are small. The results from the theory are qualitatively consistent with those of the simulations up to Pe=400. Beyond Pe=400, the distribution predicted from the theory continues to shift towards the centerline of the channel without bound, whereas the simulations indicated a limit to the extent of migration as Pe is increased. In fact, the simulation results for Pe=1100 and Pe=∞ nearly matched.[8] The limit of migration in the simulations results from hydrodynamic dispersion of a chain of point particles, similar to a sediment suspension.[22] The model of the elastic dumbbell does not include this effect.

C. Flow and force in conjunction

Application of a pressure driven flow and an external force in the same direction accentuates the migration of the polymer towards the centerline as seen in Fig. 7. For example, comparing the theoretical result for Pe=200 and $\mathrm{Pe}_f=5$ with the result for Pe=200 and $\mathrm{Pe}_f=0$ [Fig. 5(a)] shows that the depletion layer has extended from approximately $\bar{y}=1$ to $\bar{y}=1.5$ and the centerline value has increased from $n/n_t=0.32$ to $n/n_t=0.45$. Similar increases are observed in the corresponding simulation results.

The enhanced migration towards the center results only partially from the additive effect of the migration mechanisms for flow and force. Another mechanism, proportional to the cross product of the Peclet numbers is included along with the terms associated with the external force and shear-induced migration mechanisms,

$$\frac{\partial \ln[n(\bar{y})]}{\partial \bar{y}} = -\frac{\bar{a}}{8\bar{h}}\mathrm{Pe}_f^2\frac{(2\bar{y}-\bar{h})^3}{\bar{y}^2(\bar{y}-\bar{h})^2} - \frac{3\sqrt{6}\bar{a}^2\bar{h}}{320\sqrt{\pi}}\mathrm{Pe}^2\frac{2\bar{y}-\bar{h}}{\bar{y}^2(\bar{y}-\bar{h})^2} - \frac{\sqrt{6}\bar{a}}{60\sqrt{\pi}\bar{h}}\mathrm{Pe}_f\,\mathrm{Pe}(2\bar{y}-\bar{h}). \tag{71}$$

The additional contribution to the migration from the combined force and flow does not depend upon the presence of the bounding walls. As illustrated in Fig. 8, the shear flow orients the beads, on average, such that the polymer is in tension even in the bulk; the external force then causes a migration of the polymer in the direction of the average orientation, towards the center in this case. This force-induced migration of an oriented polymer is a direct result of hydrodynamic interactions between the beads.

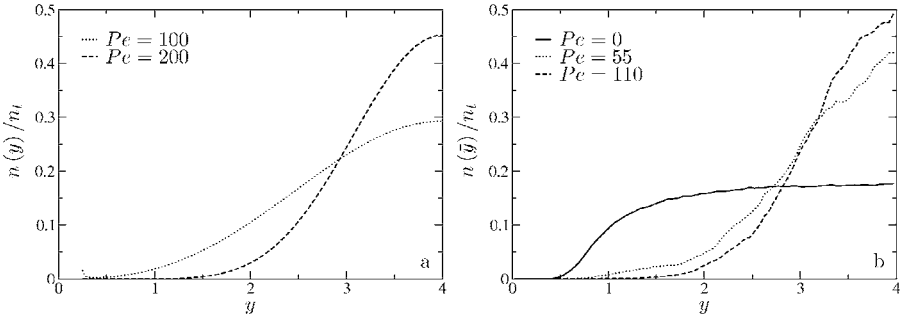

FIG. 7. Distribution $n(\bar{y})$ for the external force and flow field acting in conjunction. (a) Results from the theory are plotted at different Pe for the case of $\mathrm{Pe}_f=5$ and (b) results of numerical simulations (Ref. 8) with $\mathrm{Pe}_f=12.5$ are shown for comparison.

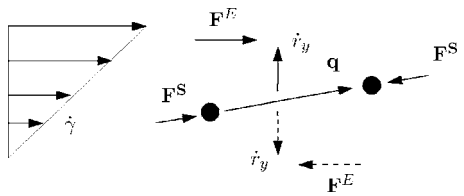

FIG. 8. The shear flow results in a preferred orientation of the polymer similar to that shown. When acting in the direction of flow, the external force (solid arrow) lifts the center-of-mass upwards (away from the wall) with velocity $\dot{r}_y$. The force, acting counter to the flow (dashed arrow), results in a drift downwards (towards the wall). Note that this mechanism does not depend upon hydrodynamic interaction with the bounding walls.

D. Flow and force in opposition

If the external force acts in the opposite direction to the flow, the direction of migration is reversed (Fig. 8). Equation (71) describes the distribution $n(\bar{y})$ modified by changing the sign of the third term,

$$\frac{\partial \ln[n(\bar{y})]}{\partial \bar{y}} = -\frac{\bar{a}}{8\bar{h}}\mathrm{Pe}_f^2\frac{(2\bar{y}-\bar{h})^3}{\bar{y}^2(\bar{y}-\bar{h})^2} - \frac{3\sqrt{6}\bar{a}^2\bar{h}}{320\sqrt{\pi}}\mathrm{Pe}^2\frac{2\bar{y}-\bar{h}}{\bar{y}^2(\bar{y}-\bar{h})^2} + \frac{\sqrt{6}\bar{a}}{60\sqrt{\pi}\bar{h}}\mathrm{Pe}_f\,\mathrm{Pe}(2\bar{y}-\bar{h}). \tag{72}$$

Consequently, there is a competition between migration to the center, arising from the independent actions of the flow field and external force, and a migration towards the wall due to the coupling of the flow field and external force.

Figure 9(a) shows results from the theory at a fixed flow rate of $\mathrm{Pe}_f=10$. For relatively small values of Pe, the maximum in the polymer distribution is closer to the bounding wall than to the centerline. As the force (Pe) increases, the maximum shifts towards the centerline. For sufficiently high Pe, the migration towards the centerline due to the applied force (the Pe^2 term) dominates the migration towards the wall resulting from the coupling of the local shear flow and drift due to the external force. Simulation results[8] [Fig. 9(b)] show a qualitatively similar behavior. The predicted transition from migration towards the wall to migration away from the wall takes place at different values of Pe and Pe_f than in the simulations.

IV. ELECTROPHORESIS

In most cases of practical interest,[10] an electric field acting upon a polyelectrolyte provides the external force. Under these conditions, screening due to the action of the applied electric field on the counterions is commonly argued to eliminate the need to consider velocity disturbances created by the electric field acting on the polymer itself.[11] However, recent visualization experiments[14,23] on DNA in the simultaneous presence of an electric field and a pressure-driven flow produced distributions similar to those appearing in Figs. 7 and 9. This observation suggests that hydrodynamic interactions created by the electric field are not fully screened. Indeed, calculations[12,13,24] based on a Debye-Hückel approximation indicate that the Green's function contains algebraically decaying terms in addition to exponentially decaying ones.

This Green's function is used here to demonstrate that complex migration behavior due to hydrodynamic interactions can still occur under electrophoresis. To enable an analytical calculation, the counterion-distribution surrounding a charged bead is assumed to have a Debye-Hückel structure despite the presence of flow. Expressions for the velocity of the center-of-mass and end-to-end vectors are developed in Sec. IV A and then applied in Sec. IV B to derive the steady state distributions, $n(\mathbf{r}_c)$ and $\psi(\mathbf{r}_c,\mathbf{q})$.

A. Velocity expressions

The external force, $Q\mathbf{E}$, is provided by an electric field, $\mathbf{E}=E\mathbf{e}_x$, acting on beads with a charge Q. Accounting for the screening of the electric field by the diffuse charge cloud of counterions, the electrophoretic mobility of a bead is given by

$$\frac{1}{\xi_e} = \frac{1}{4\pi\eta a^2\kappa}, \tag{73}$$

assuming the product, κa, of the inverse Debye length, κ, and the bead radius is large.[25] Balancing forces and neglecting inertia as in Sec. II A, the bead velocity is given by

$$\dot{\mathbf{r}}_i = \mathbf{v}_0(\mathbf{r}_i) + \mathbf{v}'(\mathbf{r}_i) + \mathbf{v}'_E(\mathbf{r}_i) + \frac{1}{\xi}(\mathbf{F}_i^B + \mathbf{F}_i^S) + \frac{1}{\xi_e}Q\mathbf{E}, \tag{74}$$

where $\mathbf{v}'$ is the velocity disturbance generated by the spring and Brownian forces [Eq. (12)] and $\mathbf{v}'_E$ is the velocity disturbance induced by the electric field $\mathbf{E}$ acting on the other bead. The electrostatic forces acting between the beads are assumed to be fully screened over the typical polymer size, $R_g \gg 1/\kappa$.[25] Likewise, the force on a bead due to the presence of a charged wall is also neglected.

The velocity disturbance induced by the electric field,

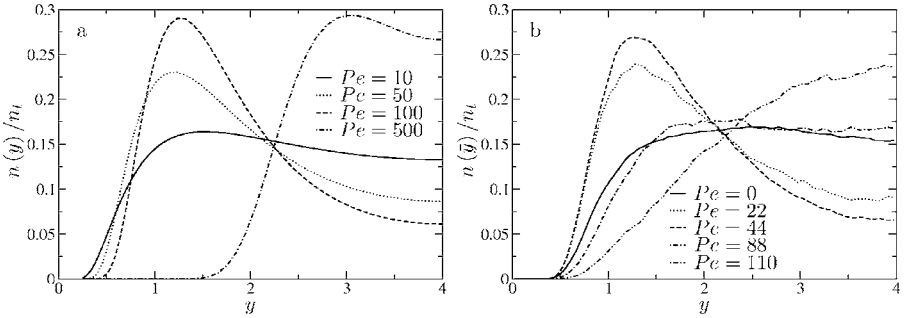

FIG. 9. Distribution $n(\bar{y})$ for an applied external force and imposed flow field acting in opposition. (a) Results of the theory for four different Pe numbers at $\mathrm{Pe}_f=10$ and (b) numerical results (Ref. 8) with $\mathrm{Pe}_f=12.5$ are shown.

$$\mathbf{v}_E'(\mathbf{r}) = \mathbf{S}^E(\mathbf{r}-\mathbf{r}_0)\cdot Q\mathbf{E}(\mathbf{r}_0), \tag{75}$$

must include the effects of screening of the velocity field by the motion of the charge cloud surrounding each bead, which is also acted upon by the electric field. Frequently, the hydrodynamic interactions are assumed to decay exponentially over a Debye length.[11] However, calculations[12,13,24] of the hydrodynamic Green's function relating the disturbance velocity at a point $\mathbf{r}$ to an electric field acting upon a screened point charge at $\mathbf{r}_0$ gives an algebraically decaying dipolar field as well as exponential terms. Retaining only the long-range dipolar term gives a hydrodynamic interaction governed by

$$\mathbf{S}^E(\mathbf{r}) = -\frac{1}{4\pi\eta\kappa^2 r^3}\left(\mathbf{I}-3\frac{\mathbf{rr}}{r^2}\right); \tag{76}$$

this is the form of the interaction used in the subsequent calculations. Note that this interaction tensor does not account for the presence of the walls.

Using Eq. (76) within Eq. (74) gives the velocity of a bead,

$$\dot{\mathbf{r}}_i = \mathbf{v}_0(\mathbf{r}_i) + \sum_{j=1}^{2}\left[\left(\mathbf{\Omega}_{ij}+\frac{\delta_{ij}}{\xi}\mathbf{I}\right)\cdot(\mathbf{F}_j^B+\mathbf{F}_j^S) + \left(\mathbf{S}_{ij}^E+\frac{\delta_{ij}}{\xi_e}\mathbf{I}\right)\cdot Q\mathbf{E}\right], \tag{77}$$

where $\mathbf{S}_{ij}^E=\mathbf{S}^E(\mathbf{r}_i-\mathbf{r}_j)$ if $i\neq j$ and equals zero if $i=j$. Similarly to Eqs. (18) and (19), the velocity of the center-of-mass and connector vector are

$$\dot{\mathbf{r}}_c = \mathbf{v}_0(\mathbf{r}_c) + \frac{1}{8}\mathbf{qq}:\nabla\nabla\mathbf{v}_0 + \frac{1}{2}\bar{\mathbf{\Omega}}\cdot\mathbf{F}^S + \bar{\mathbf{S}}^E\cdot Q\mathbf{E} + \frac{k_BT}{2}\bar{\mathbf{\Omega}}\cdot\frac{\partial\ln(\Psi)}{\partial\mathbf{q}} - \mathbf{D}_K\cdot\frac{\partial\ln(\Psi)}{\partial\mathbf{r}_c}, \tag{78}$$

$$\dot{\mathbf{q}} = \mathbf{q}\cdot\nabla\mathbf{v}_0 - \left(\frac{2}{\xi}\mathbf{I}+\hat{\mathbf{\Omega}}\right)\cdot\mathbf{F}^S - k_BT\left(\frac{2}{\xi}\mathbf{I}+\hat{\mathbf{\Omega}}\right)\cdot\frac{\partial\ln(\Psi)}{\partial\mathbf{q}} + \frac{k_BT}{2}\bar{\bar{\mathbf{\Omega}}}\cdot\frac{\partial\ln(\Psi)}{\partial\mathbf{r}_c}, \tag{79}$$

where

$$\bar{\mathbf{S}}^E = \mathbf{S}^E(\mathbf{q}) + \frac{1}{\xi_e}\mathbf{I} \tag{80}$$

and the electric field does not rotate or stretch the polymer (no contribution to $\dot{\mathbf{q}}$).

B. Probability distribution

Substituting Eqs. (78) and (79) into Eqs. (4) and (7) gives equations for the center-of-mass distribution and end-to-end distribution functions, $n(y_c)$ and ψ. As in Eq. (31), the flux in the y-direction,

$$n\langle\dot{\mathbf{r}}_c\rangle\cdot\mathbf{e}_y = \frac{\lambda}{2}nH\langle q_x^2-2q_y^2+q_z^2\rangle + nQE\langle S_{yx}^E\rangle - \frac{nk_BT}{2}\frac{\partial}{\partial y_c}\langle S_{yy}\rangle - \frac{k_BT}{2\xi}[1+\xi\langle S_{yy}\rangle - 2\omega(y_c)]\frac{\partial n}{\partial y_c}, \tag{81}$$

vanishes at steady state. Calculating the ensemble averages appearing in Eq. (81) requires a solution of the equation for the orientation distribution,

$$0 = \dot{\gamma}q_y\frac{\partial\psi}{\partial q_x} - \frac{2H}{\xi}\left(3\psi+\mathbf{q}\cdot\frac{\partial\psi}{\partial\mathbf{q}}\right) - \frac{2k_BT}{\xi}\frac{\partial^2\psi}{\partial\mathbf{q}^2}. \tag{82}$$

As in Eq. (33), the contributions of $\hat{\mathbf{\Omega}}$ and $\bar{\bar{\mathbf{\Omega}}}$ have been ignored and a Hookean spring force has been used. Due to the fact that $\bar{\mathbf{S}}^E$ does not include the asymmetry arising from interactions with the walls, the electric field does not affect the end-to-end distribution. As a result, this theory will not predict migration arising from the electric field alone.

The solution of Eq. (82) is

$$\psi(y,\mathbf{q}) = \frac{1}{J}\exp\left[-\frac{1}{2d_3}((q_x^*)^2 + d_1q_x^*q_y^* + d_2(q_y^*)^2 + d_3(q_z^*)^2)\right], \tag{83}$$

with coefficients

$$d_1 = -\tfrac{1}{2}\dot{\gamma}^*, \tag{84}$$

$$d_2 = 1+\tfrac{1}{8}(\dot{\gamma}^*)^2, \tag{85}$$

$$d_3 = 1+\tfrac{1}{16}(\dot{\gamma}^*)^2, \tag{86}$$

and normalization factor

$$J = \left[\frac{2\pi k_BT}{H}\right]^{3/2}\left[\frac{4d_3^2}{4d_2-d_1^2}\right]^{1/2}. \tag{87}$$

Expanding Eq. (83) about $\dot{\gamma}^*=0$ to second order gives

$$\psi(y,\mathbf{q}) = \psi_{\mathrm{eq}}\left[1+\frac{1}{4}\dot{\gamma}^*q_x^*q_y^* + \frac{1}{32}(\dot{\gamma}^*)^2(-1-(q_y^*)^2+(q_x^*)^2 + (q_x^*q_y^*)^2)\right], \tag{88}$$

from which the ensemble averages in Eq. (81) are calculated. The results are

$$\langle q_x^2-2q_y^2+q_z^2\rangle = \left(\frac{k_BT}{H}\right)\frac{1}{8}(\dot{\gamma}^*)^2, \tag{89}$$

$$\langle S_{yy}\rangle = \left(\frac{1}{\eta}\sqrt{\frac{H}{k_BT}}\right)\frac{1}{840(2\pi)^{3/2}}[560-11(\dot{\gamma}^*)^2], \tag{90}$$

$$\langle S_{yx}^E\rangle = \left(\frac{1}{\eta}\sqrt{\frac{H}{k_BT}}\right)\frac{1}{20(2\pi)^{3/2}}(\kappa^*)^{-2}\dot{\gamma}^*, \tag{91}$$

where

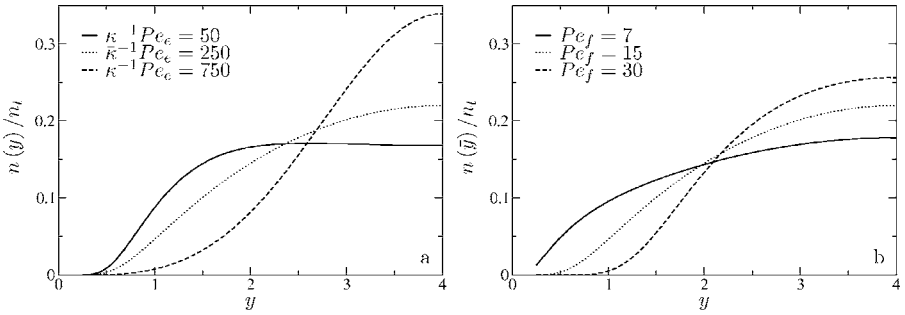

FIG. 10. Distribution $n(\bar{y})$ for the electrophoretic and pressure-driven flow acting in conjunction. Results are shown for (a) $\mathrm{Pe}_f=15$ and (b) $\bar{\kappa}^{-1}\,\mathrm{Pe}_e=250$.

$$\kappa^* = \sqrt{\frac{k_B T}{H}}\kappa. \tag{92}$$

For a pressure-driven flow, the y-dependent value of the shear rate, $\dot{\gamma}^*$, is given by Eq. (34).

C. Center-of-mass distribution

Setting $n\langle \dot{\mathbf{r}}_c\rangle \cdot \mathbf{e}_y$ to zero in Eq. (81) and using the ensemble averages as calculated in Eqs. (89)–(91) gives an equation governing the distribution for the center-of-mass,

$$\mathcal{D}_e^* \frac{\partial \ln[n(y^*)]}{\partial y^*} = \mathcal{S}_e^* + \mathcal{F}_e^* + \mathcal{G}_e^*, \tag{93}$$

where

$$\mathcal{D}_e^* = 1 + \frac{a^*}{280\sqrt{2\pi}}[560 - 11(\dot{\gamma}^*)^2] - \frac{9a^*h^*}{4y^*(y^* - h^*)}, \tag{94}$$

$$\mathcal{S}_e^* = \frac{3\pi}{4}a^*\lambda^*(\dot{\gamma}^*)^2, \tag{95}$$

$$\mathcal{F}_e^* = \frac{1}{10(2\pi)^{3/2}}\frac{F_e^*\dot{\gamma}^*}{(\kappa^*)^2}, \tag{96}$$

$$\mathcal{G}_e^* = \frac{11}{280\sqrt{2\pi}}a^*\frac{\partial}{\partial y^*}(\dot{\gamma}^*)^2 \tag{97}$$

and F_e^* has been defined as

$$F_e^* = \frac{\xi QE}{\eta k_B T}. \tag{98}$$

Note that the expressions for $\mathcal{D}_e^*$, $\mathcal{S}_e^*$, and $\mathcal{G}_e^*$ match those for $\mathcal{D}^*$, $\mathcal{S}^*$, and $\mathcal{G}^*$ [Eqs. (52), (53), and (55)], but with F^* set to zero. The primary difference with the previous result of Eq. (51) appears in Eq. (96) for $\mathcal{F}_e^*$. This term includes the effect of the screening of the hydrodynamic interactions, as apparent from the quadratic dependence on the Debye length, $1/\kappa^*$.

To compare with results presented in Sec. III, Eq. (93) is rewritten in terms of the Peclet numbers. The nondimensional parameters $\bar{a}$, $\bar{h}$, $\bar{y}$, and Pe_f have been defined as in Sec. II C. The inverse Debye length is nondimensionalized by the radius of gyration,

$$\bar{\kappa} = \kappa R_g, \tag{99}$$

and the Peclet number, Pe_e, due to the electric field acting on the charged polymer, is defined as

$$\mathrm{Pe}_e = \frac{R_g u_e}{D_0} = \frac{3\sqrt{3}QE}{2(k_B T H)^{1/2}\kappa a}, \tag{100}$$

where $u_e = QE/\xi_e$ is the electrophoretic velocity of the free draining dumbbell. Equation (93) becomes

$$\bar{\mathcal{D}}_e \frac{\partial \ln[n(\bar{y})]}{\partial \bar{y}} = \bar{\mathcal{S}}_e + \bar{\mathcal{F}}_e + \bar{\mathcal{G}}_e, \tag{101}$$

where

$$\bar{\mathcal{D}}_e = 1 + \sqrt{\frac{3\bar{a}^2}{2\pi}}\left[1 - \frac{11}{315\bar{h}^2}\mathrm{Pe}_f^2(2\bar{y} - \bar{h})\right] - \frac{9\bar{a}\bar{h}}{4}\frac{1}{\bar{y}(\bar{y} - \bar{h})}, \tag{102}$$

$$\bar{\mathcal{S}}_e = -\frac{\bar{a}}{8\bar{h}}\mathrm{Pe}_f^2\frac{(2\bar{y} - \bar{h})^3}{\bar{y}^2(\bar{y} - \bar{h})^2}, \tag{103}$$

$$\bar{\mathcal{F}}_e = \mp \frac{\sqrt{6}\bar{a}^2}{80\sqrt{\pi}\bar{h}}(\bar{\kappa}^{-1}\mathrm{Pe}_e)\mathrm{Pe}_f(2\bar{y} - \bar{h}), \tag{104}$$

$$\bar{\mathcal{G}}_e = \frac{22\sqrt{6}\bar{a}}{315\sqrt{\pi}\bar{h}^2}\mathrm{Pe}_f^2(2\bar{y} - \bar{h}). \tag{105}$$

In Eq. (104), the minus corresponds to the case of electrophoresis in the same direction as the flow field and the plus for electrophoresis opposing the flow direction. The quadratic dependence of $\bar{\mathcal{F}}_e$ on the Debye length is no longer explicit, since the definition of Pe_e contains one factor of $\bar{\kappa}^{-1}$.

D. Results

The calculations of Sec. III were repeated for identical conditions, substituting electrophoresis for the body force. The channel width is $\bar{h}=8$ and the bead radius is $\bar{a}=0.125$. For the results shown, the value of $n(\bar{y})$ is set to zero near the wall by performing the integration between $\bar{y}=0.25$ and $\bar{h}-0.25$; the diffusivity, $\bar{\mathcal{D}}_e$, is set to 1 in Eq. (101).

When the electrophoretic force acts in the same direction as the pressure-driven flow, the dumbbell migrates toward the center of the channel as seen in Fig. 10. The hydrody-

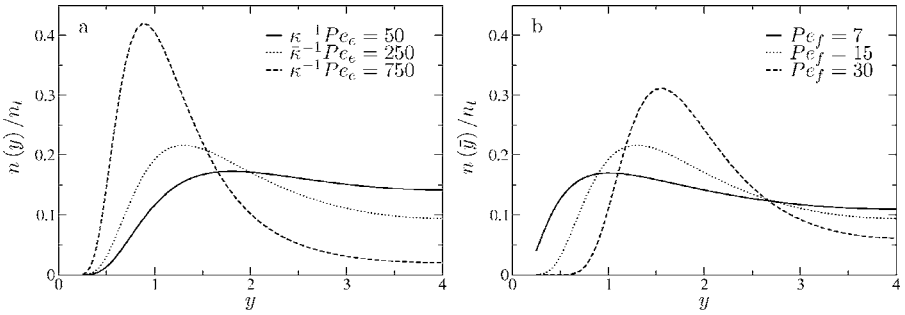

FIG. 11. Distribution $n(\bar{y})$ for the electrophoretic and pressure-driven flow acting in opposition. Results are shown for (a) $\mathrm{Pe}_f=15$ and (b) $\bar{\kappa}^{-1}\,\mathrm{Pe}_e=250$.

namic interactions induced by the electric field create an additional migration flux away from the wall, which enhances the probability distribution at the centerline beyond that observed for pressure-driven flow alone. However, if these interactions were screened on the Debye length scale, the data in Fig. 10(a) would collapse onto a single curve matching the results in Fig. 4 for $\mathrm{Pe}_f=15$ and $\mathrm{Pe}=0$. Ignoring the velocity disturbances induced by the electric field sets $\langle S^E_{yx}\rangle$ to zero and eliminates contributions of the electric field to the transverse flux in Eq. (81). Consequently, $\bar{\mathcal{F}}_e$ within Eq. (101) would become zero and reduce the solution for the distribution $n(\bar{y})$ to that given by Eq. (68), which includes only the effects of the pressure-driven flow. Physically, the enhanced migration towards the center of the channel is caused by a mechanism qualitatively similar to the one discussed in Sec. III C and illustrated in Fig. 8. The shear flow aligns the polymer, which then drifts in the applied electric field due to the dipolar hydrodynamic interactions between the beads. This coupling is approximated by the term $nQE\langle S^E_{yx}\rangle$ in Eq. (81).

Migration towards the center, under the combined action of flow and electrophoresis, has been observed experimentally,[14] but neither flow nor electrophoresis produced significant migration in isolation. In the laboratory experiments,[14] the channel was much wider in comparison to the polymer size, $h\sim 100R_g$, and the flow rate was small, $\mathrm{Pe}_f<10$. Under these conditions, migration driven by hydrodynamic interactions with the walls is small and the dominant contribution comes from the coupling between the rotated and stretched polymer and the dipolar disturbance field. The physics in the laboratory experiments are contained within a simplified version of Eq. (101),

$$\frac{\partial \ln[n(\bar{y})]}{\partial \bar{y}} = -\frac{\sqrt{6}\bar{a}^2}{80\sqrt{\pi}\bar{h}}(\bar{\kappa}^{-1}\,\mathrm{Pe}_e)\mathrm{Pe}_f(2\bar{y}-\bar{h}). \tag{106}$$

To observe the more complex behavior predicted by the theory, the experiments should be repeated in narrow channels, $h\sim 10R_g$.

Further evidence that the disturbances induced by the electric field are not fully screened is obtained by reversing the direction of the electrophoretic motion. Upon reversal, Zheng and Yeung[14] observed migration of the polymer towards the wall, which is consistent with the physical picture presented in Fig. 8 and as argued in Sec. III D for the case of an external force in the absence of any screening. For electrophoretic motion opposing the direction of flow, the current theory can predict migration towards the bounding wall only if the hydrodynamic interactions induced by the electric field are retained. Figure 11(a) shows the result of the calculation. Increasing $\bar{\kappa}^{-1}\,\mathrm{Pe}_e$ increases the maximum value of $n(\bar{y})$ and moves the maximum towards the bounding walls at $\bar{y}=0$.

Zheng and Yeung[14] suggested that the mechanism shown in Fig. 8 was responsible for the migration behavior observed in their experiments, specifically discussing migration of an ellipsoidal particle. However, they did not address screening of the hydrodynamic interactions, which can potentially eliminate the coupling between the applied electric field and the migration velocity. For example, rigid dumbbells[26] and slender rods[27] with a uniform charge distribution on the surface of the particle and an infinitely thin double layer experience no transverse motion in response to an applied electric field, regardless of the orientation of the particle.

Figure 11(a) shows that the maximum value of $n(\bar{y})$ continues to increase and shift towards the wall as $\bar{\kappa}^{-1}\,\mathrm{Pe}_e$ increases. This contrasts with the previous case (Fig. 9) of a body force, where the maximum shifted towards the center for a sufficiently high forcing. In the current case, the interactions of the applied forces with the bounding walls are not included in the analysis, therefore a reversal is not predicted. However, migration towards the center is observed for sufficiently large flow rates. As seen in Fig. 11(b), the maximum increases and shifts towards the center with increasing Pe_f while holding $\bar{\kappa}^{-1}\,\mathrm{Pe}_e$ constant.

V. CONCLUSIONS

The cross-stream migration of a confined polymer, driven by combinations of external force and flow fields, has been examined using the kinetic theory of a dumbbell. The results qualitatively reproduce the distributions calculated from multibead numerical simulations[4,8] of polymers in pressure-driven and centrifugal fields. Lack of quantitative agreement arises from the simplifications within the theory and the reduced conformational degrees of freedom of the dumbbell. The simplifications included superposing the far-field approximation for the hydrodynamic interactions with the bounding walls, assuming that the orientation distribution depends only parametrically on the position of the center-of-mass, and approximating the orientation distribution by a power series in the force and flow fields. Nevertheless, the theory clearly identifies the mechanisms causing migration. For the case of a pressure-driven flow, the inhomogeneous distribution results from the previously identified effects of

gradients in diffusivity[21] and shear-induced migration.[7] With an external force, but no flow, a preferential orientation induced by the presence of the walls and a subsequent drift away from the walls creates a net migration towards the center. Coupling between shear-induced orientation of the polymer and the external force can cause either migration towards the center or towards the walls, depending upon the direction of the force.

Taken together, these mechanisms enable considerable control of the distribution of the polymer transverse to the flow direction. However, in electrical fields the additional complications associated with counterion screening must be considered. Consequently, extensions to the theory were made to account for screening of the hydrodynamic interactions by the counterions. Simplifying assumptions, in addition to those listed above, included using the Debye-Hückel approximation and ignoring disturbances of the counterion distribution due to the flow field. The theory predicts migration of the polymer in agreement with recent experimental observations,[14,23] indicating that the hydrodynamic interactions induced by the electric field in polyelectrolytes are not fully screened.

ACKNOWLEDGMENTS

This work was supported by the National Science Foundation Grant No. CTS-0505929.

APPENDIX: HYDRODYNAMIC INTERACTIONS OF A DUMBBELL WITH A PLANAR BOUNDARY

In this section we derive the corrections to the mobility tensors of a dumbbell due to the presence of a planar boundary. We consider the Green's function $\mathbf{G}(\mathbf{r},\mathbf{r}_0)$ for the hydrodynamic interactions between a dumbbell and a planar no-slip boundary, in the limit that the separation between the beads $\mathbf{q}$ is small compared to the distance of the center-of-mass $\mathbf{r}_c$ from the wall.

We consider a dumbbell with beads located at $\mathbf{r}_c-\mathbf{q}/2$ and $\mathbf{r}_c+\mathbf{q}/2$, and expand $\mathbf{G}(\mathbf{r}_c\mp\mathbf{q}/2,\mathbf{r}_c\mp\mathbf{q}/2)$ with $|\mathbf{q}|\ll y_c$ in a Taylor series about $\mathbf{q}=0$. To linear order in $\mathbf{q}$,

$$\mathbf{G}(\mathbf{r}_c\mp\mathbf{q}/2,\mathbf{r}_c\mp\mathbf{q}/2) = \mathbf{G}(\mathbf{r}_c,\mathbf{r}_c)\mp\frac{\mathbf{q}}{2}\cdot\frac{\partial}{\partial\mathbf{r}}\mathbf{G}(\mathbf{r},\mathbf{r}_c)\Big|_{\mathbf{r}=\mathbf{r}_c} \mp\frac{\mathbf{q}}{2}\cdot\frac{\partial}{\partial\mathbf{r}_0}\mathbf{G}(\mathbf{r}_c,\mathbf{r}_0)\Big|_{\mathbf{r}_0=\mathbf{r}_c}, \tag{A1}$$

where the minus sign is associated with bead 1 and the plus sign with bead 2. The wall contributions to the hydrodynamic mobilities defined in Eqs. (20)–(23) are then calculated to linear order in $\mathbf{q}$,

$$\mathbf{G}_K = \mathbf{G}(\mathbf{r}_c,\mathbf{r}_c), \tag{A2}$$

$$\bar{\mathbf{G}} = -2\mathbf{q}\cdot\frac{\partial}{\partial\mathbf{r}_0}\mathbf{G}(\mathbf{r}_c,\mathbf{r}_0)\Big|_{\mathbf{r}_0=\mathbf{r}_c}, \tag{A3}$$

$$\hat{\mathbf{G}} = 0, \tag{A4}$$

$$\bar{\bar{\mathbf{G}}} = -2\mathbf{q}\cdot\frac{\partial}{\partial\mathbf{r}}\mathbf{G}(\mathbf{r},\mathbf{r}_c)\Big|_{\mathbf{r}=\mathbf{r}_c}. \tag{A5}$$

In what follows, we only consider the Green's function, $\mathbf{G}_0$, for a planar wall located at $y=0$. The Green's function for two walls, Eq. (13), is then obtained by superposition $\mathbf{G}=\mathbf{G}_0+\mathbf{G}_h$.

If we define the vector $\mathbf{R}$ from the image source, located at $\mathbf{r}_0-2y_0\mathbf{e}_y$, to the field point $\mathbf{r}$,

$$\mathbf{R} = \mathbf{r}-\mathbf{r}_0+2y_0\mathbf{e}_y, \tag{A6}$$

then the single-wall Green's function is

$$\mathbf{G}_0(\mathbf{r},\mathbf{r}_0) = -\mathbf{S}(\mathbf{R})+2y_0^2\mathbf{P}^D(\mathbf{R})-2y_0\mathbf{S}^D(\mathbf{R}), \tag{A7}$$

with the Stokeslet, dipole, and doublet contributions given most compactly in Cartesian tensor form,

$$S_{\alpha\beta}(\mathbf{R}) = \frac{1}{8\pi\eta}\left(\frac{\delta_{\alpha\beta}}{R}+\frac{R_\alpha R_\beta}{R^3}\right), \tag{A8}$$

$$P^D_{\alpha\beta}(\mathbf{R}) = \frac{sg(\beta)}{8\pi\eta}\left(\frac{\delta_{\alpha\beta}}{R^3}-\frac{3R_\alpha R_\beta}{R^5}\right), \tag{A9}$$

$$S^D_{\alpha\beta}(\mathbf{R}) = R_y P^D_{\alpha\beta}(\mathbf{R})+\frac{sg(\beta)}{8\pi\eta}\left(\frac{R_\alpha\delta_{\beta y}-R_\beta\delta_{\alpha y}}{R^3}\right). \tag{A10}$$

The function $sg(\beta)$ is $+1$ for the components $\beta=x$ and $\beta=z$, and -1 when $\beta=y$.

When the source and field points are both at the center of mass of the dumbbell, $\mathbf{R}=2y_c\mathbf{e}_y$, the Stokeslet, dipole, and doublet are

$$S_{\alpha\beta}(2y_c\mathbf{e}_y) = \frac{1}{16\pi\eta y_c}(\delta_{\alpha\beta}+\delta_{\alpha y}\delta_{\beta y}), \tag{A11}$$

$$P^D_{\alpha\beta}(2y_c\mathbf{e}_y) = \frac{1}{64\pi\eta y_c^3}(\delta_{\alpha\beta}+\delta_{\alpha y}\delta_{\beta y}), \tag{A12}$$

$$S^D_{\alpha\beta}(2y_c\mathbf{e}_y) = \frac{1}{32\pi\eta y_c^2}(\delta_{\alpha\beta}+\delta_{\alpha y}\delta_{\beta y}), \tag{A13}$$

where the following relations were used to simplify the Kronecker delta functions,

$$sg(\beta)\delta_{\alpha\beta} = \delta_{\alpha\beta}-2\delta_{\alpha y}\delta_{\beta y}, \tag{A14}$$

$$sg(\beta)\delta_{\alpha y}\delta_{\beta y} = -\delta_{\alpha y}\delta_{\beta y}. \tag{A15}$$

Combining the results in Eqs. (A11) and (A12), we obtain the contribution to the Kirkwood mobility, D_K/k_BT, from the wall at $h=0$,

$$\mathbf{G}_{0K} = -\frac{3}{32\pi\eta y_c}(\mathbf{I}+\mathbf{e}_y\mathbf{e}_y). \tag{A16}$$

The gradients of $\mathbf{G}_0$ can be calculated using the translational invariance of the Green's function with respect to the location of the field point and the image source [Eq. (A6)],

$$\frac{\partial}{\partial\mathbf{r}_\alpha} = \frac{\partial}{\partial\mathbf{R}_\alpha} = \nabla_\alpha, \tag{A17}$$

$$\frac{\partial}{\partial \mathbf{r}_{0\alpha}} = -sg(\alpha)\nabla_\alpha. \tag{A18}$$

The remaining nonzero mobility matrices, $\bar{\mathbf{G}}$ and $\bar{\bar{\mathbf{G}}}$ are then,

$$\bar{\mathbf{G}}_0 = -sg(\gamma)\,(2q_\gamma \nabla_\gamma S_{\alpha\beta} - 4y_c^2 q_\gamma \nabla_\gamma P^D_{\alpha\beta} + 4y_c q_\gamma \nabla_\gamma S^D_{\alpha\beta})|_{\mathbf{R}=2y_c\mathbf{e}_y}, \tag{A19}$$

$$\bar{\bar{\mathbf{G}}}_0 = (2q_\gamma \nabla_\gamma S_{\alpha\beta} - 4y_c^2 q_\gamma \nabla_\gamma P^D_{\alpha\beta} + 4y_c q_\gamma \nabla_\gamma S^D_{\alpha\beta})|_{\mathbf{R}=2y_c\mathbf{e}_y}. \tag{A20}$$

The expression for $\bar{\mathbf{G}}_0$ contains two additional terms, $-8y_c q_y P^D_{\alpha\beta}(2y_c\mathbf{e}_y) + 4q_y S^D_{\alpha\beta}(2y_c\mathbf{e}_y)$, but they exactly cancel, as can be seen from Eqs. (A12) and (A13).

Finally we need to calculate the gradients of the Stokeslet, dipole, and doublet terms, again using the results of Eqs. (A14) and (A15),

$$\nabla_\gamma S_{\alpha\beta}(\mathbf{R})|_{\mathbf{R}=2y_c\mathbf{e}_y} = \frac{1}{32\pi\eta y_c^2}(-\delta_{\alpha\beta}\delta_{\gamma y} + \delta_{\alpha\gamma}\delta_{\beta y} + \delta_{\beta\gamma}\delta_{\alpha y} - 3\delta_{\alpha y}\delta_{\beta y}\delta_{\gamma y}), \tag{A21}$$

$$\nabla_\gamma P^D_{\alpha\beta}(\mathbf{R})|_{\mathbf{R}=2y_c\mathbf{e}_y} = \frac{3}{128\pi\eta y_c^4}(-\delta_{\alpha\beta}\delta_{\gamma y} + \delta_{\alpha\gamma}\delta_{\beta y} - \delta_{\beta\gamma}\delta_{\alpha y} - \delta_{\alpha y}\delta_{\beta y}\delta_{\gamma y}), \tag{A22}$$

$$\nabla_\gamma S^D_{\alpha\beta}(\mathbf{R})|_{\mathbf{R}=2y_c\mathbf{e}_y} = \frac{1}{32\pi\eta y_c^3}(-\delta_{\alpha\beta}\delta_{\gamma y} + \delta_{\alpha\gamma}\delta_{\beta y} - 2\delta_{\beta\gamma}\delta_{\alpha y}). \tag{A23}$$

These results can be combined to give the expressions for $\bar{\mathbf{G}}_0$ and $\bar{\bar{\mathbf{G}}}_0$,

$$\bar{\mathbf{G}}_0 = -\frac{3}{32\pi\eta y_c^2}[(\mathbf{I} + \mathbf{e}_y\mathbf{e}_y)q_y - \mathbf{e}_y\mathbf{q} + \mathbf{q}\mathbf{e}_y], \tag{A24}$$

$$\bar{\bar{\mathbf{G}}}_0 = -\frac{3}{32\pi\eta y_c^2}[(\mathbf{I} + \mathbf{e}_y\mathbf{e}_y)q_y + \mathbf{e}_y\mathbf{q} - \mathbf{q}\mathbf{e}_y]. \tag{A25}$$

After superposing the contribution from the upper wall, we obtain the expressions for $\bar{\mathbf{G}}$ and $\bar{\bar{\mathbf{G}}}$ given in Eqs. (25) and (27). In fact $\bar{\mathbf{G}}$ and $\bar{\bar{\mathbf{G}}}$ are the matrix transpose of one another. The results for $\mathbf{G}_K$ and $\bar{\mathbf{G}}$ agree with the results of Ma and Graham.[7]

[1] U. Agarwal, A. Dutta, and R. Mashelkar, "Migration of macromolecules under flow: The physical origin and engineering implications," Chem. Eng. Sci. **49**, 1693 (1994).
[2] R. Jendrejack, D. Schwartz, J. dePablo, and M. Graham, "Shear-induced migration in flowing polymer solutions: Simulation of long-chain DNA in microchannels," J. Chem. Phys. **120**, 2513 (2004).
[3] J. Hernandez-Ortiz, H. Ma, J. dePablo, and M. Graham, "Cross-stream-line migration in confined flowing polymer solutions: Theory and simulation," Phys. Fluids **18**, 123101 (2006).
[4] O. B. Usta, J. E. Butler, and A. Ladd, "Flow-induced migration of polymers in dilute solution," Phys. Fluids **18**, 031703 (2006).
[5] L. Fang, H. Hu, and R. Larson, "DNA configurations and concentration in shearing flow near a glass surface in a microchannel," J. Rheol. **49**, 127 (2005).
[6] D. Saintillan, E. Shaqfeh, and E. Darve, "Effect of flexibility on the shear-induced migration of short-chain polymers in parabolic channel flow," J. Fluid Mech. **557**, 297 (2006).
[7] H. Ma and M. Graham, "Theory of shear-induced migration in dilute polymer solutions near solid boundaries," Phys. Fluids **17**, 083103 (2005).
[8] O. B. Usta, J. E. Butler, and A. Ladd, "Transverse migration of a confined polymer driven by an external force," Phys. Rev. Lett. **98**, 098301 (2007).
[9] J. Zheng and E. Yeung, "Mechanism for the separation of large molecules based on radial migration in capillary electrophoresis," Anal. Chem. **75**, 3675 (2003).
[10] J.-L. Viovy, "Electrophoresis of DNA and other polyelectrolytes: Physical mechanisms," Rev. Mod. Phys. **72**, 813 (2000).
[11] G. Manning, "Limiting laws and counterion condensation in polyelectrolyte solutions. 7. Electrophoretic mobility and conductance," J. Chem. Phys. **85**, 1506 (1981).
[12] D. Long and A. Ajdari, "A note on the screening of hydrodynamic interactions in electrophoresis and in porous media," Eur. Phys. J. E **4**, 29 (2001).
[13] D. Long, J.-L. Viovy, and A. Ajdari, "Simultaneous action of electric fields and nonelectric forces on a polyelectrolyte: Motion and deformation," Phys. Rev. Lett. **76**, 3858 (1996).
[14] J. Zheng and E. Yeung, "Anomalous radial migration of single DNA molecules in capillary electrophoresis," Anal. Chem. **74**, 4536 (2002).
[15] R. Bird, C. Curtiss, R. Armstrong, and O. Hassager, *Dynamics of Polymeric Liquids*, 2nd ed. (Wiley, New York, 1987), Vol. 2.
[16] J. Happel and H. Brenner, *Low-Reynolds Number Hydrodynamics* (Martinus Nijhoff, Dordrecht, 1986).
[17] N. Liron and S. Mochon, "Stokes flow for a Stokeslet between two parallel flat plates," J. Eng. Math. **10**, 287 (1976).
[18] J. Blake, "A note on the image system for a Stokeslet in a no-slip boundary," Proc. Cambridge Philos. Soc. **70**, 70 (1971).
[19] N. Hoda and S. Kumar, "Kinetic theory of polyelectrolyte adsorption in shear flow," J. Rheol. **51**, 799 (2007).
[20] R. Armstrong, "Kinetic theory and rheology of dilute solutions of flexible macromolecules. 1. Steady state behavior," J. Chem. Phys. **60**, 724 (1974).
[21] G. Sekhon, R. Armstrong, and M. Jhon, "The origin of polymer migration in a non-homogeneous flow field," J. Polym. Sci., Polym. Phys. Ed. **20**, 947 (1982).
[22] R. Caflisch and J. Luke, "Variance in the sedimentation speed of a suspension," Phys. Fluids **28**, 759 (1985).
[23] E. Yeung, "Dynamics of single biomolecules in free solution," Annu. Rev. Phys. Chem. **55**, 97 (2004).
[24] S. Allison and D. Stigter, "A commentary on the screened-Oseen counterion-condensation formalism of polyion electrophoresis," Biophys. J. **78**, 121 (2000).
[25] W. B. Russel, S. Saville, and W. Schowalter, *Colloidal Dispersions* (Cambridge University Press, New York, 1989).
[26] M. Fair and J. Anderson, "Electrophoresis of dumbbell-like colloidal particles," Int. J. Thermophys. **16**, 663 (1990).
[27] Y. Solomentsev and J. Anderson, "Electrophoresis of slender particles," J. Fluid Mech. **279**, 197 (1994).